V European Conference on Computational Fluid Dynamics
ECCOMAS CFD 2010
J. C. F. Pereira and A. Sequeira (Eds)
Lisbon, Portugal,14-17 June 2010

IMPLEMENTATION OF A 3D COMPRESSIBLE MHD SOLVER ABLE TO MODEL TRANSONIC FLOWS

Carlos M. Xisto*, José C. Páscoa†, Paulo J. Oliveira† and Davide A. Nicolini††

*†University of Beira Interior,
Electromechanical Engineering Department R. Mq.s DÁvila e Bolama, 6201-001 Covilhã, Portugal
e-mail: xisto@ubi.pt, pascoa@ubi.pt, pjpo@ubi.pt
††European Space Agency
Directorate of Science and Robotic Exploration ESTEC, Keplerlaan 1, 2201AZ Noordwijk, The Netherlands
e-mail: davide.nicolini@esa.int

Key words: MHD, compressible flow, OpenFOAM

Abstract. *The modeling of transonic flow using a pressure based solver is here tackled with the PISO method, in particular with the rhoPISOFoam code. This code has been applied for a wide range of Mach numbers in order to evaluate its limits under high speed flow conditions. Computations are obtained for canonical geometries and the results are compared with those obtained with the FLUENT code, in regard to efficiency and computing cost. Most results to be discussed are for the prototypical geometry of a channel with a semicircular bump. In view of the good results obtained with rhoPISOFoam we decided to implement a new algorithm capable of solving compressible MHD flows. Flow fields obtained using a transverse magnetic field under a constant electric potential wall turned out to exhibit attenuation of the shock wave, allowing for a better recuperation of the flow downstream of the bump. We also present results for a blunt body MHD flow. A bow shock is computed for a supersonic flow impinging on a perfectly conducting cylinder with, and without, an applied magnetic field. We see this new solver as an initial step into modeling MHD compressible flows, such as those existent in MPD thrusters.*

1 INTRODUCTION

In order to develop high-power space propulsion systems research has been targeted toward the acceleration of plasma flows, namely for efficient conversion of exit enthalpy in MPD thrusters[1]. The Eulerian field Mach number can assume values ranging from the very low subsonic to the order of 10. In Applied-Field MPD[2] thrusters the plasma flows are accelerated by an imposed magnetic field. To completely describe a plasma motion we must rely on kinetic equations for each of the plasma species. However, to model MPD thrusters this approach is often too costly and therefore herein we resort to a fluid description of the plasma. This is usually done by solving the MHD equations using a single fluid approach based either on a one or two temperature model, for ions and electrons. The mathematical model presented in this work comprises the solution of the single fluid resistive MHD equations. In spite of being one of the simplest models to describe this class of flows, it is one of the approaches that has been met with most success when applied to simulate the physics of these propulsion engines. Therefore here whe shall solve the gas dynamic equations coupled to the magnetic field induction equation.

For compressible flows one of the most popular approaches is to solve the governing equations in conservative variables using a finite volume method. But inside realistic geometries the flowfield can assume values ranging from the low subsonic to the hypersonic limit. For classical gas dynamics, the use of standard density based methods to model low Mach number flowfields usually implies a reduction in the numerical efficiency, due to the increased stiffness of the equations and weak coupling between density and pressure. This has been often mitigated by using low Mach-preconditioning[3], but that implies an additional computational cost.

Alternatively, to tackle flows at all speeds, finite volume segregated pressure based solvers have been applied. These were initially developed for incompressible flow using the SIMPLE pressure-velocity coupling algorithm, however they have already been proved as capable of handling flows in all flow regimes, including computing shock wave discontinuities[4]. Herein we will consider the PISO variant[5,6]. Various versions have been developed to compute compressible flow, mainly differing in the formulation for the pressure equation. Further, and as a way to reduce the computing time, this pressure-velocity coupling algorithm has been reformulated to achieve faster execution time in a parallel computing framework[7]. The algorithm used in the present computations is applied on the OpenFOAM-Open Field Operation and Manipulation toolbox[8,9]. A brief review of the algorithm will be given in section 3. Further, we will present computations that allow us to verify the ability of the code to compute transonic and supersonic flows with shock wave discontinuities.

The computation of high speed flowfields using an MHD formulation is further complicated by the imposition of a magnetic field. A consequence of Faraday's law is that an initially divergence free magnetic field leads to a divergence free magnetic field at all times. This is reflected on the absence of observations of magnetic monopoles in nature.

This solenoidal property is expressed as $\nabla \cdot \mathbf{B}$, and presents one of the main challenges to be taken into considerations when modeling MHD plasma flows[3,10].

The present work includes a complete description of the governing equations in Section 2, the presentation of the numerical algorithm developed to compute MHD compressible flows in Section 3, a presentation of two test cases used to check the code in Section 4, and finally a conclusions section.

2 GOVERNING EQUATIONS

We solve the MHD equations expressed in the conservative variables, density ρ, momentum vector $\rho\mathbf{U}$, total energy density ρe, and magnetic induction $\mathbf{B}$. The system of equations is given by,

$$\frac{\partial \rho}{\partial t} + \nabla \cdot (\rho \mathbf{U}) = 0, \tag{1}$$

$$\frac{\partial \rho \mathbf{U}}{\partial t} + \nabla \cdot (\rho \mathbf{U}\mathbf{U}) = -\nabla p \mathcal{I} + \nabla \cdot \tau_{visc} + \mathbf{J} \times \mathbf{B}, \tag{2}$$

where τ_{visc} is the viscous stress tensor and the last term in r.h.s, $\mathbf{J} \times \mathbf{B}$, is the Lorentz force. We now consider the Maxwell equations,

$$\nabla \times \mathbf{H} = \mathbf{J} + \frac{\partial \mathbf{D}}{\partial t}, \quad \nabla \times \mathbf{E} = -\frac{\partial \mathbf{B}}{\partial t}, \quad \nabla \cdot \mathbf{B} = 0, \quad \nabla \cdot \mathbf{J} = 0. \tag{3}$$

The magnetic field intensity is $\mathbf{H} = \mathbf{B}/\mu_0$, and $\mathbf{D}$ is the displacement current that is neglected for non-relativistic plasma computations. $\mathbf{E}$ is the electric field and $\mathbf{J}$ the current density. Using vector identities and the Maxwell equations (3) we can replace this force by a set of stresses:

$$\mathbf{J} \times \mathbf{B} = \nabla \cdot \left(\frac{\mathbf{B}\mathbf{B}}{\mu_0} - \frac{B^2}{2\mu_0} \mathcal{I} \right), \tag{4}$$

where $\mathcal{I}$ is the identity tensor. Now we can rewrite the momentum equation:

$$\frac{\partial \rho \mathbf{U}}{\partial t} + \nabla \cdot (\rho \mathbf{U}\mathbf{U}) = \nabla \cdot \tau_{visc} - \nabla \left(p + \frac{B^2}{2\mu_0} \right) + \nabla \cdot \left(\frac{\mathbf{B}\mathbf{B}}{\mu_0} \right). \tag{5}$$

The overall pressure is given by $P_{ove.} = p + B^2/2\mu_0$, in which the second contribution corresponds to the magnetic pressure. This later acts like a pressure in the direction transverse to the magnetic field, the magnetic field resists to compressibility just like the fluid pressure. The term $\mathbf{B}\mathbf{B}/\mu_0$ in equation (5) is called the hoop stress and acts like a tension along the lines of magnetic force, bearing some similarity with the viscous stresses. It represents tension along field lines when they are curved, similar to the force exerted by a stretched elastic band.

Combining Faraday's law $\nabla \times \mathbf{E} = -\frac{\partial \mathbf{B}}{\partial t}$ with the Ohm's law, $\mathbf{J} = \sigma(\mathbf{E} + \mathbf{U} \times \mathbf{B})$, we obtain

$$\frac{\partial \mathbf{B}}{\partial t} = \nabla \times (\mathbf{U} \times \mathbf{B}) + \frac{1}{\mu_0 \sigma} \nabla^2 \mathbf{B}, \tag{6}$$

were the first term in the r.h.s. is the convective term and the second one is the diffusion term. The relationship between these two terms allow us to obtain the magnetic Reynolds number, $R_m = \mu_0 \sigma L u$, where μ_0 is the magnetic permeability, σ is the conductivity, L and u are the characteristic length and velocity respectively. This is a parameter that we must considerer in the modeling assumptions for MHD flows. In the case of $R_m \leq 1$ the electromagnetic forces are ruled by the flowfield and the convective and dissipative terms must be retained in the induction equation. In the case of a high magnetic Reynolds number ($R_m \gg 1$) we may neglected the diffusion term, but we end up with a strong coupling, so the momentum, Ohm's law, energy equation and induction equation cannot be treated independently. For the case of a low magnetic Reynolds number ($R_m \ll 1$) we may neglected the convective term and we can treat each equation separately introducing the contributions of the magnetic field only as a source term. In our case we will retain the diffusion and convective terms in the induction equation, thus solving for the more general case of a strong coupling between equations.

Additionally, and in particular for compressible MHD flows, we have to solve the energy equation,

$$\frac{\partial (\rho e)}{\partial t} + \nabla \cdot (\rho e \mathbf{U}) + \nabla \cdot (P_{ove.} \mathbf{U}) - \nabla \cdot (\alpha \nabla e) - \frac{1}{\mu_0} \nabla \cdot (\mathbf{B} (\mathbf{B} \cdot \mathbf{U})) - \nabla \cdot (\mathbf{B} \times \eta \mathbf{J}) = 0 \tag{7}$$

Let us now concentrate in the last term of the equation, $\nabla \cdot (\mathbf{B} \times \eta \mathbf{J})$, and $\eta \mathbf{J} = \frac{\eta}{\mu_0} \nabla \times \mathbf{B}$, assuming a constant resistivity and that $\eta = \frac{1}{\mu_0 \sigma}$ this term can then be re-writen as:

$$\nabla \cdot (\mathbf{B} \times \eta \mathbf{J}) = \nabla \cdot \left[\frac{1}{\mu_0 \sigma} (\mathbf{B} \times (\nabla \times \mathbf{B})) \right] = \nabla^2 \left(\frac{1}{2 \mu_0^2 \sigma} B^2 \right) - \frac{1}{\mu_0^2 \sigma} [\nabla \cdot (\nabla \cdot (\mathbf{B}\mathbf{B}))] \tag{8}$$

This later is substituted in the last term of Eq. (7).

The numerical code will thus compute a solution to the compressible MHD flowfield by solving Eq.s (1), (5), (6) and (7).

3 NUMERICAL MODEL

The algorithm herein presented will extend the incompressible MHD algorithm[8], available in OpenFOAM, to compressible flow. The solution of the governing equations will be obtained using a finite volume discretization that solves the equations in a segregated approach. Thus, the flow variables will remain frozen as we solve for the other variables at a given time step. The code solves for velocity, pressure, total energy, and magnetic field. This procedure is sub-divided into two phases. In the first we solve a pressure equation

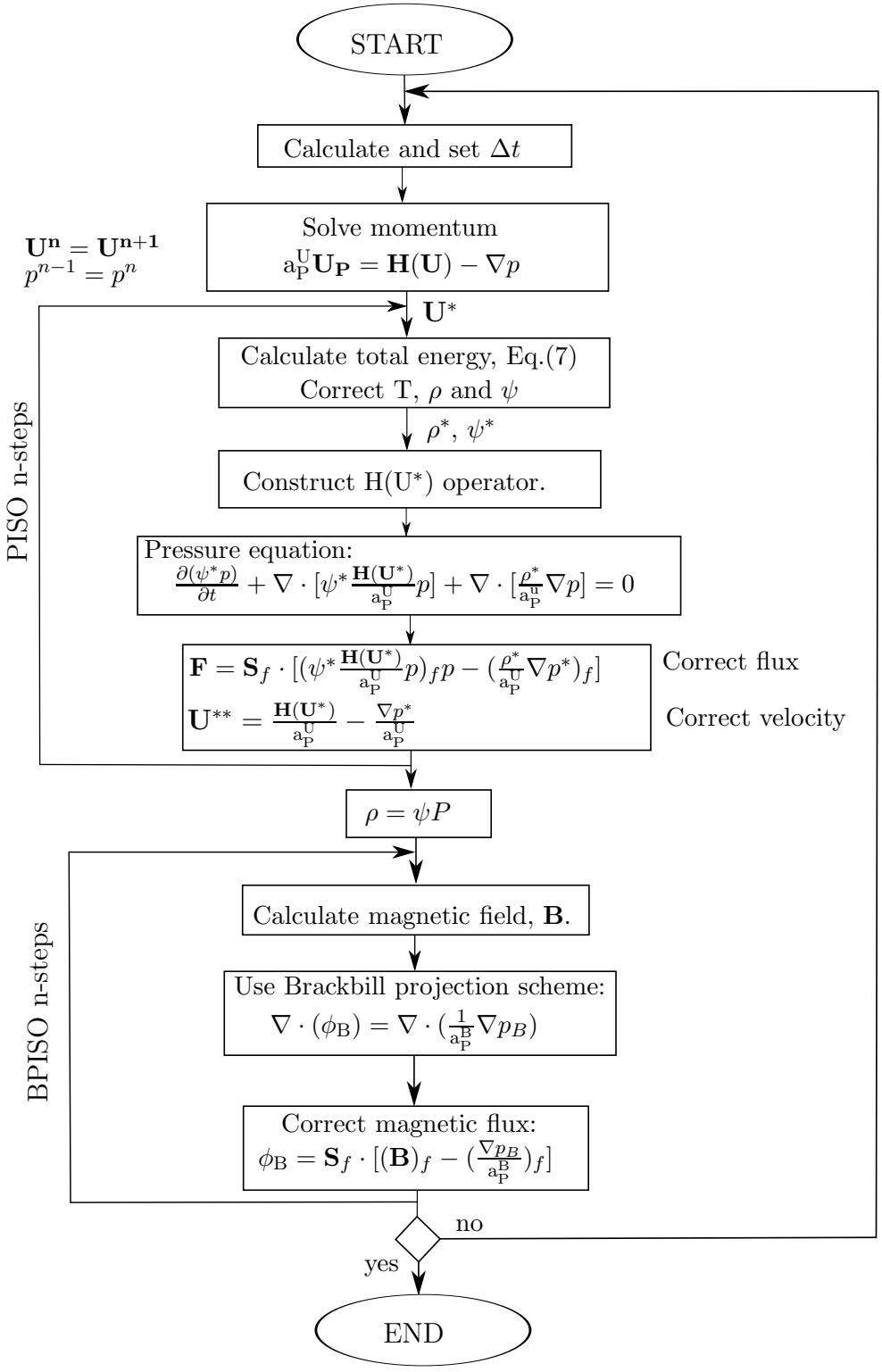

Figure 1: Fluxogram corresponding to the new solver for MHD compressible flow.

using the PISO implementation for all flow speeds[6]. On a second phase we solve for the induction equation, further ensuring that the irrotationality condition $\nabla \cdot \mathbf{B} \approx 0$ is meet. This later is accomplished using the projection method of Brackbill and Barnes[10]. The flowchart of the coded algorithm is presented in Fig.1.

The implemented algorithm comprises the following steps:

1. *Momentum predictor:* The estimated values at the present time step for the velocity field, $\mathbf{U}^*$, are obtained by solving the momentum equation. The pressure gradient and the magnetic field terms are treated in an explicit way, using the values of the previous time step. This is an initial step before we start the PISO cycle.

2. Inside the PISO cycle we solve for the total energy, and afterwards the temperature T is updated using a state equation;

$$T = \frac{1}{\rho C_v}\left[\rho e - \frac{1}{2}\rho U^2 - \frac{1}{2\mu_0}B^2\right]. \tag{9}$$

   On the other hand the compressibility, $\psi^* = 1/RT^*$, and density, $\rho^* = \psi^* P$, are also estimated.

3. The operator $\mathbf{H}(\mathbf{U}^*)$ is constructed by using the estimated values for velocity. This term will be used for the solution of the pressure equation in the next step. The magnetic field values are taken from the previous time step.

4. *Pressure equation:* The presure equation, see Fig.1, is solved using the first estimates for compressibility, ψ^*, and density, ρ^*, in order to obtain an estimated pressure, p^*. Several non-orthogonality steps are performed for non-orthogonal meshes.

5. *Correct flux and Velocity:* By using the estimated pressure the flux can now be corrected and we proceed to correct the velocity. The correction for velocity, $\mathbf{U}^{**}$ is performed in an explicit way using the new pressure gradient, ∇p^* and the first predicted velocity, $\mathbf{U}^* = \mathbf{H}(\mathbf{U}^*)/\mathrm{a_P^U}$.

6. *Density correction:* When all the pre-defined steps for PISO are performed we make a last correction for density using the final pressure. These steps should be sufficient for the continuity equation to be satisfied. Therefore the continuity equation is effectvely introduced inside the PISO cycle and it is possible to check the mass conservation error. For this, we use the density obtained from continuity equation and compare with the value obtained with state equation $\rho = \psi p$.

7. We now proceed to the magnetic component of the algorithm. The magnetic field is computed from the induction equation, and we ensure the solenoidal nature of the magnetic field using the projection method. The method guaranties $\nabla \cdot \mathbf{B} \approx 0$ by correcting the computed magnetic field. The BPISO name comes from the idea

that the $\nabla \cdot \mathbf{B}^*$ field provided by a PISO similar scheme in the $n+1$ time step is projected into a divergence free $\nabla \cdot \mathbf{B}^{n+1}$ field. Assuming the flow is sufficiently smooth the magnetic vector field can be decomposed into the sum of a curl and a gradient, $\mathbf{B}^* = \nabla \times \mathbf{A} + \nabla\phi$. Here the curl of the vector potential $\mathbf{A}$ contains the real physical part of $\mathbf{B}^*$. Applying the divergence to both sides we obtain a Poisson equation, $\nabla^2\phi = \nabla \cdot \mathbf{B}^*$, that can be solved for the scalar function ϕ. We finally obtain the physical meaningful magnetic field $\mathbf{B}^{n+1} = \mathbf{B}^* - \nabla\phi$. This step is accomplished using the same MHD algorithm implemented in OpenFOAM for incompressible flow[8]. In the magnetic field equation is introduced a fictitious magnetic-flux pressure to prescribe the solenoidal constraint, in a similar way as the pressure equation in a classical PISO scheme. At convergence, this variable is of the order of the discretization error.

4 RESULTS

This section presents results obtained with the code described in the previous sections. We have initially started by incorporating the compressible gas dynamics solver into the existing incompressible MHD version of the code. We proceed with the incorporation of the magnetic component in order to obtain a full working MHD compressible solver. To test the gas dynamic implementation we resort to the well known bump channel flow, see Moukalled and Darwish[11]. A second test case is also presented corresponding to a perfectly conducting cylinder under supersonic MHD flow conditions, see Sjögreen and Yee[12].

4.1 Numerical analysis on the effect of the magnetic field on shock damping

Results are presented for pure gas dynamic and also for MHD flow. In these later conditions a shock wave damping arises, see e. g. Vatazhin *et. al*[13].

In Fig.2 it is depicted a 3D view of the mesh used to perform the computation, and the corresponding boundary conditions. The length of the bump is equal to the channel height, and its thickness is ten percent of the channel height. Although this test case has no analytical solution it has been widely used to check the precision and stability of related numerical codes. A mesh refinement study was performed and comparison is also conducted with a solution obtained using a density based solver of the FLUENT commercial code, see Fig.3.

For the pure gas dynamic problem the following boundary conditions are considered: at inlet we impose temperature and total pressure; at outlet we impose static pressure. All the remaining variables are extrapolated from the domain. Further we consider an uniformly distributed magnetic field and solid walls are considered isolated walls by imposing the magnetic field B_0. Results are obtained for inviscid flow using the Gamma scheme[9] for convective term treatment.

In Fig.4 we present results for the shock wave damping due to the imposition of two

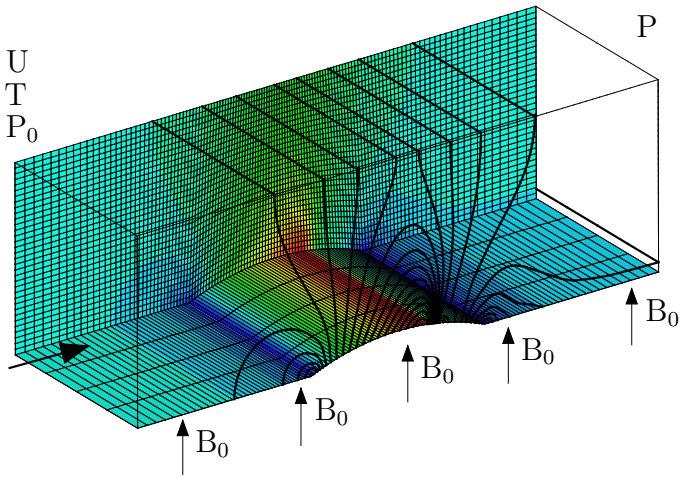

Figure 2: A 3D view of the mesh and corresponding boundary conditions.

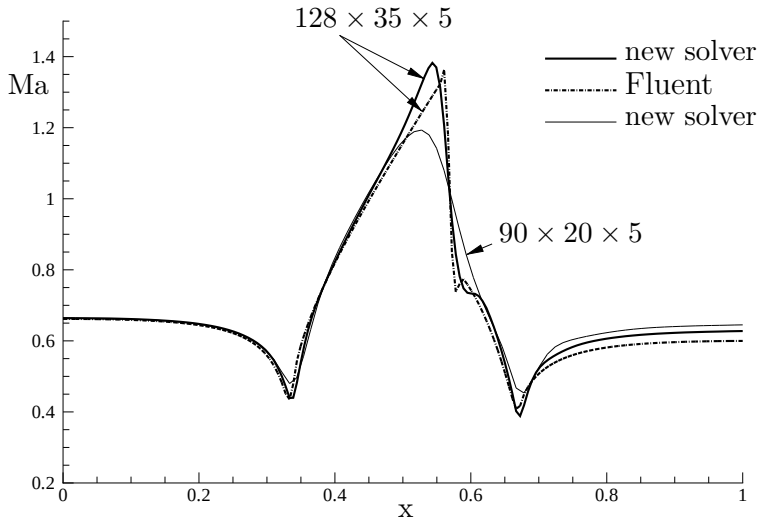

Figure 3: Comparison between the results obtained with Fluent and the new solver($B_0 = 0$). Mach number evolution for the mid-span section of the channel.

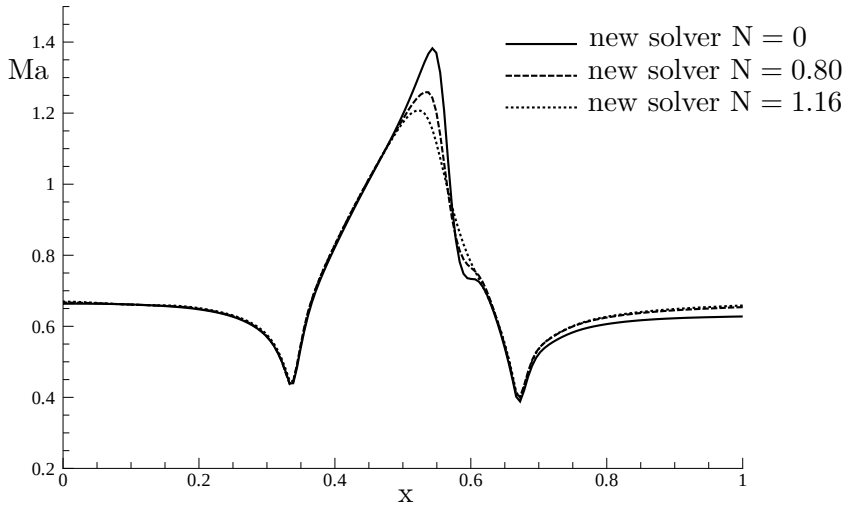

Figure 4: Shock wave damping under a imposed magnetic field, B_0. Here $N = \sigma B^2 L/\rho u$ is the interaction parameter, a measure of the relative weights of Lorentz and inertial forces. The interaction parameter can also be seen as the ratio of the damping time, $\tau = \rho/\sigma B^2$, to the characteristic advection time, L/u.

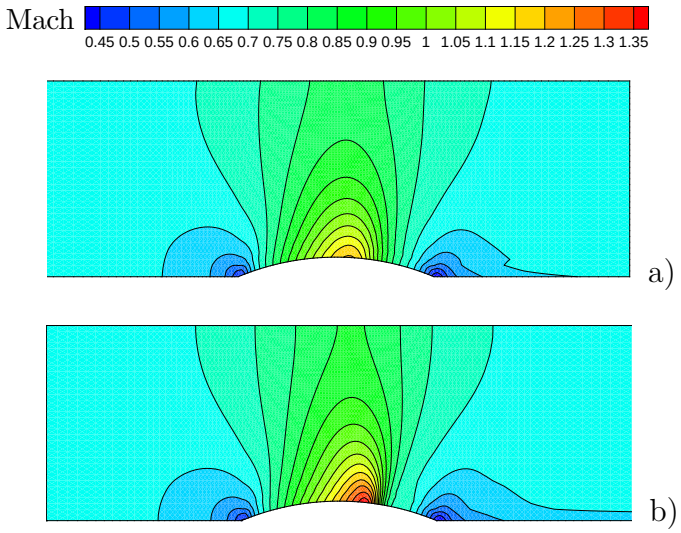

Figure 5: Comparison between the results obtained for the Mach flowfield; a) with and b) without an imposed magnetic field.

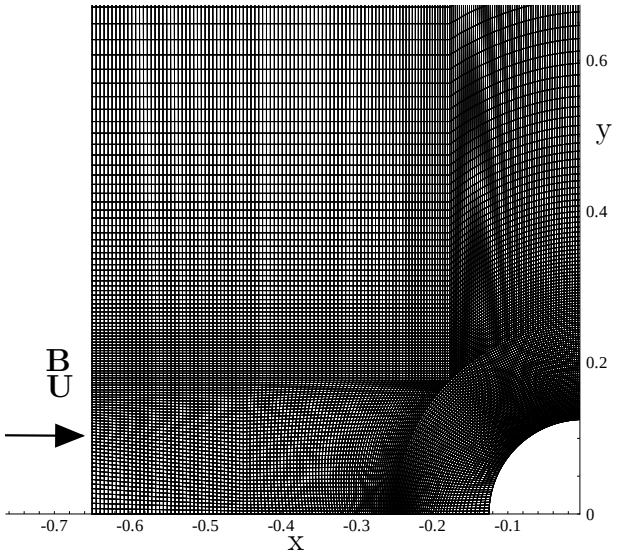

Figure 6: Partial 2D view of the mesh used and imposed boundary conditions.

transversal magnetic fields. These results are for a magnetic Reynolds number, at inlet, of $R_m \approx 20$ and for two interaction parameters, namely N = 0.8 e N = 1.16.

It is clearly visible that, in the pure gas dynamic problem, a shock wave appears slightly downwind from the top of the bump. After applying a transversal magnetic field the shock wave intensity and position are changed. There is a redistribution of the flow in order to comply with the continuity condition on a vertical section at that location. This is clearly visible by an increase in the area which is between mach number contours, slightly larger for the case of an imposed magnetic field, see Fig.5. This kind of damping has been the subject of intensive research, namely for applications regarding hypersonic propulsion[14].

4.2 Blunt body MHD flow

This is a very tough test case that has called the interest of several researchers[12,14]. The occurance of exotic MHD discontinuities is influenced by the inlet velocity and fluid β. Here $\beta = 2p/B^2$ relates pure gas dynamic and magnetic forces, namely for $\beta >> 1$ the pure gas dynamic forces govern the flow and for $\beta << 1$ the flow is controlled by magnetic forces.

In Fig.6 we present a portion of the mesh emploied and the corresponding boundary conditions. The computational domain comprises a rectangular region above the upper left quadrant of a cylinder, extending to $x = -0.65$ along x-axis, and to $y = -1.4$ along y-axis. A 2D structured mesh, with 160×120 nodes, is used for the computations. No mesh independence study has been performed yet, but we have used a mesh with similar refinement to that of De Sterck[13]. A MUSCL scheme was used to treat the convective terms.

In Fig.7 we present the results obtained for the MHD flow on a conducting cylinder.

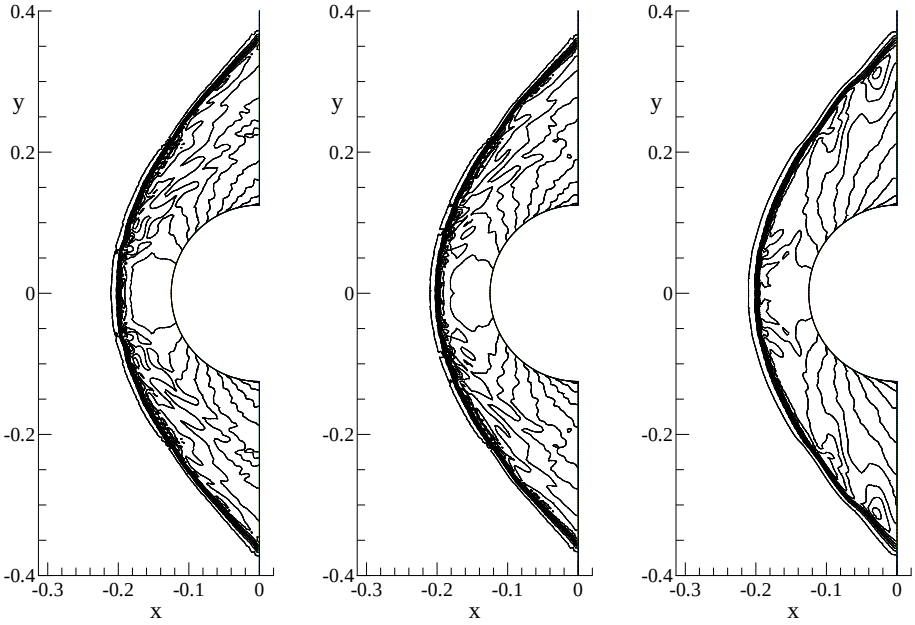

(a) Ideal MHD $\beta = 5$.

(b) Ideal MHD $\beta = 10$.

(c) Ideal MHD $\beta = 10$, with Gamma.

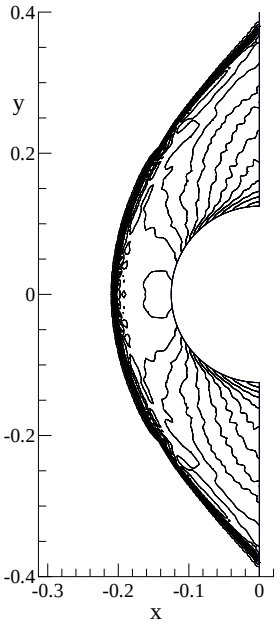

(d) Resistive ($\sigma = 100$), viscous ($Re = 1000$) MHD $\beta = 5$.

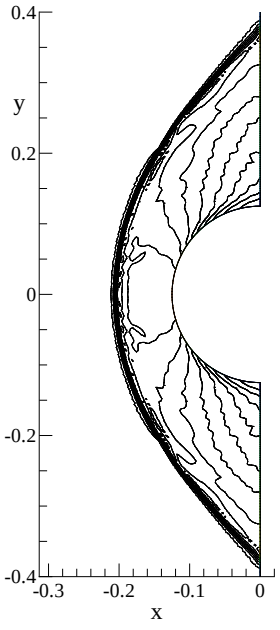

(e) Resistive ($\sigma = 100$), viscous ($Re = 1000$) MHD $\beta = 10$.

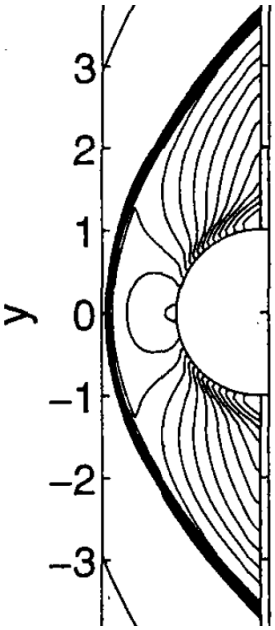

(f) Resistive ($\sigma = 100$), viscous ($Re = 1000$) MHD $\beta = 5$, Sjögree and Yee[12].

Figure 7: Results obtained for the density contours, for computation of the MHD supersonic flow impinging on a perfectly conducting cylinder.

The presented results depict the changes occurring in the flowfield as we switch from the MHD ideal model, for $\beta = 5$ and $\beta = 10$, to a resistive MHD computation for $\sigma = 100$ and $Re = 1000$. It is observed that the position, and shape, of the shock wave changes as we move from an ideal to a resistive computation (Joule effect). There are no significative changes, regarding the position and shape of the shock wave, for the ideal MHD solutions obtained for different β values. Furthermore, we have been working towards obtaining a solution for conditions of low β (namely $\beta < 1$) but, for the time being, results have been unsuccessful.

However, the most worrisome fact of these contour plots is the presence of wiggles, which are similar to those observed in the odd-even decoupling of velocity and pressure on colocated meshes. We are now trying to understand the cause for this problem, while at the same time testing other high-resolution differencing schemes for the convective terms in the transport equations.

5 CONCLUSIONS

The main objective of the present work was to present the developments attained on the course of the implementation of an MHD compressible flow solver. Also, numerical computations for two distinct geometries under conditions of pure gas dynamic and MHD flow were carried out and are discussed.

The results obtained for a 3D channel with a bump were compared against results obtained with the Fluent code, and some minor discrepancies are visible. It should be mentioned that the Fluent computations are based on a density based solver, whereas our results are based on a pressure based solver. This can be a main cause of discrepancies in results. In spite of this fact, additional simulations with better differencing schemes for the convective terms should be further investigated.

One of the toughest test cases that can be found in the literature concerns the supersonic flow impinging on a cylinder body, subjected to an imposed magnetic field. Several conditions are considered, including laminar flow computation with joule effect dissipation. Results are compared with reference literature solutions. Problems of stability of computations where found for low values of β. Also, the results obtained with MUSCL present an oscillatory behavior, with the Gamma limiter giving much better results. However, the problem of wiggles in these solution fields also requires further investigation.

6 ACKNOWLEDGMENT

This work was supported by FCT grant SFRH/BD/60285/2009. Additional financial support was provided by CAST- Center for Aerospace Science and Technology at UBI.

REFERENCES

[1] S. Roy, P. Mikellides and D. R. Reddy, Effective conversion of exit enthalpy in a MPD thruster, *AIAA-Paper 2002-0917*, In proceedings of the *40th Aerospace Sci-*

ences Meeting and Exhibit (1991).

[2] J. Páscoa, F. Brójo, J. Monteiro, Numerical Simulation of Magneto-plasma Thrusters for Aerospace Propulsion Using an MHD Formulation, *Paper O-7.2*, In proceedings of the *14th International Conference on Emerging Nuclear Energy Systems,* (2009).

[3] D. R. van der Heul, C. Vuik and P. Wesseling, A conservative pressure-based correction method for the Euler and ideal MHD equations at all speeds, *Int. J. Num. Meth. Fluids*, **40**, 521–529 (2002).

[4] M. Darbandi, E. Roohi and V. Mokarizadeh, Conceptual Linearization of Euler Governing Equations to Solve High Speed Compressible Flow Using a Pressure-Based Method, *Numerical Methods for Partial Differential Equations*, **24**(2), 583–604 (2008).

[5] R. I. Issa, Solution of the implicitly discretized fluid flow equations by operator-splitting, *Journal of Computational Physics*, **62**, 40–65 (1986).

[6] R. I. Issa and M. H. Javareshkian, Pressure-based compressible calculation method utilizing total variation diminishing schemes, *AIAA Journal*, **36**, 1652–1657 (1998).

[7] N. W. Bressloff, A parallel pressure implicit splitting of operators algorithm applied to flows at all speeds, *Int. J. Numer. Methods Fluids*, **36**, 497–617 (2001).

[8] H. G. Weller, G. Tabor, H. Jasak and C. Fureby, A Tensorial Approach to CFD using Object Orientated Techniques, *Computers in Physics*, **12**(6), 620–631 (1998).

[9] H. Jasak, H. G. Weller, A. D. Gosman, High resolution NVD differencing scheme for arbitrarily unstructured meshes, *Int. J. Numer. Meth. Fluids*, **31**, 431–449 (1999).

[10] J. U. Brackbill, D. C. Barnes, The effect of nonzero $\nabla \cdot b$ on the numerical solution of the magnetohydrodynamic equations, *J. Comput. Phys*, **35**, 426–430 (1980).

[11] F. Moukalled, M. Darish, A high-resolution pressure-based algorithm for fluid flow at all speeds, *J. Comput. Phys*, **168**, 101–133 (2001).

[12] B. Sjögreen, H. C. Yee, Numerical study of resistivity and Hall effects for a compresssible MHD model, *AIAA-Paper 5046-2005*, In proceedings of the *36th Plasmadynamics and Lasers Conference* (2005).

[13] A. B. Vatazhin, O. V. Gouskov, V. I. Kopchenov, The investigation of supersonic flow deceleration by magnetic field, *Vol. 3*-13, In proceedings of the *13th. International Conference on MHD Electrical Power Generation and High Temperature Technologies*, The International Liaison Group on MHD energy conversion, 875–883 (1999).

[14] H. De Sterck, H. Deconinck, S. Poedts, D. Roose, A bow shock flow containing (almost) all types of (exotic) MHD discontinuities, In proceedings of the *Seventh International Conference on Hyperbolic Problems: Theory, Numerics, Applications, Int. Series of Numerical Mathematics* 129–195 (1999).